



1 **Modelled variations of the inherent optical properties of summer** 2 **Arctic ice and their effects on the radiation budget: A case based on** 3 **ice cores from CHINARE 2008–2016**

4 Miao Yu¹, Peng Lu¹, Matti Leppäranta², Bin Cheng³, Ruibo Lei⁴, Bingrui Li⁴, Qingkai Wang¹, Zhijun Li¹

5 ¹State Key Laboratory of Coastal and Offshore Engineering, Dalian University of Technology, Dalian, China

6 ²Institute of Atmosphere and Earth Sciences, University of Helsinki, Helsinki, Finland

7 ³Finnish Meteorological Institute, Helsinki, Finland

8 ⁴MNR Key Laboratory for Polar Science, Polar Research Institute of China, Shanghai, China

9 *Corresponding to:* Peng Lu (lupeng@dlut.edu.cn), Zhijun Li (lizhijun@dlut.edu.cn).

10 **Abstract.** Variations in Arctic sea ice are not only apparent in its extent and thickness but also in its internal properties under
11 global warming. The microstructure of summer Arctic sea ice changes due to varying external forcing, ice age, and extended
12 melting seasons, which affect its optical properties. Sea ice cores sampled in the Pacific sector of the Arctic obtained by the
13 Chinese National Arctic Research Expeditions (CHINARE) during the summers of 2008 to 2016 were used to estimate the
14 variations in the microstructures and inherent optical properties (IOPs) of ice and determine the radiation budget of sea ice
15 based on a radiative transfer model. Compared with 2008, the volume fraction of gas bubbles in the top layer of sea ice in
16 2016 increased by 7.5%, and decreased by 50.3% in the interior layer. Meanwhile, the volume fraction of brine pockets
17 increased clearly in the study years. The changing microstructure resulted in an increase in the scattering coefficient in the top
18 ice layers by 9.3% from 2008 to 2016, while an opposite situation occurred in the interior layer. These estimated ice IOPs fell
19 within the range of other observations and their variations were related to increasing air temperature and decreasing ice ages.
20 At the Arctic basin scale, the changing IOPs of ice greatly changed the amount of solar radiation transmitted to the upper ocean
21 even when a constant ice thickness is assumed, especially in marginal ice zones, implying the presence of different sea ice
22 bottom melt processes. These findings revealed the important role of the changing IOPs of ice in affecting the radiation transfer
23 of Arctic sea ice.

24 **1 Introduction**

25 The recent rise in air temperature in the Arctic is almost twice the global average, known as Arctic amplification (Dai et
26 al., 2019), which has been seen in the retreat of sea ice, especially in summer. The extent of sea ice in summer has decreased
27 (Comiso et al., 2008; Parkinson & Comiso, 2013; Petty et al., 2018), and summer ice is thinner (Kwok, 2018), younger
28 (Stroeve and Notz, 2018), and warmer (Wang et al., 2020) than before. These changes have affected the transfer of sunlight
29 into the Arctic Ocean, and the optical properties of sea ice are changing the solar radiation budget in the area.



30 Variations of Arctic sea ice cover are related not only to the macroscale properties described above but also to the ice
31 microstructure. Sea ice is a multiphase medium consisting of pure ice, gas bubbles, brine pockets, salt crystals, and sediments
32 (Hunke et al., 2011). In the last decades, the length of the Arctic ice melt season has shown a significant positive trend (Markus
33 et al., 2009), and the Arctic ice cover has experienced a transition from predominantly old ice to primarily first-year ice
34 (Stroeve and Notz, 2018; Tschudi et al., 2020). At the same time, in melting ice gas bubbles and brine pockets tend to become
35 larger (Light et al., 2003), and phase changes due to brine salinity and temperature result in variations in the volume of gas and
36 brine (Weeks and Ackley, 1986; Crabeck et al., 2019). Therefore, the physical properties of ice have changed and in the past
37 10 years the bulk density of summer Arctic sea ice has been lower than reported in the 1990s due to increased ice porosity
38 (Wang et al., 2020).

39 Gas bubbles and brine pockets, as dominant optical scatterers, directly influence the inherent optical properties (IOPs) of
40 sea ice (Grenfell, 1991; Perovich, 2003). IOPs include scattering and absorption coefficients and information about the phase
41 function of the domain. The varying IOPs of ice have attracted attention due to their important role in the ice–albedo feedback
42 process. Light et al. (2008) and Katlein et al. (2019; 2021) demonstrated clear IOPs variations during the melting season, and
43 difference in the IOPs between first-year ice and multiyear ice have been ascertained in many observations (e.g., Light et al.,
44 2015; Grenfell et al., 2006). There are also differences in the IOPs of first-year ice because of different stages of melting
45 (Veysière et al., 2022). Yu et al. (2022) carried out a study to investigate the sensitivity of ice IOPs on its microstructures, but
46 they did not show how the ice IOPs change in the real world. Changes in ice microstructure and IOPs are especially important
47 for the Arctic under the general warming climate and decreasing ice age. Even in the latest studies and sea ice models, IOPs are
48 set as constants based on previous field observations (e.g., Briegleb & Light, 2007), which is somewhat in contrast to the
49 reality in the Arctic Ocean.

50 In this study, *in situ* observations of the physical properties of summer Arctic sea ice during the Chinese National Arctic
51 Research Expeditions (CHINARE) from 2008 to 2016 were employed as input data. Variations of the microstructure and IOPs
52 of Arctic sea ice are presented. Also shown are their quantitative effects on the radiation budget in the area. Applying these
53 varying IOPs to satellite-observed sea ice conditions has allowed us to obtain Arctic-wide estimates of role of ice’s
54 microstructure in the radiation budget of the region.

55 **2 Data and method**

56 **2.1 Arctic sea ice coring**

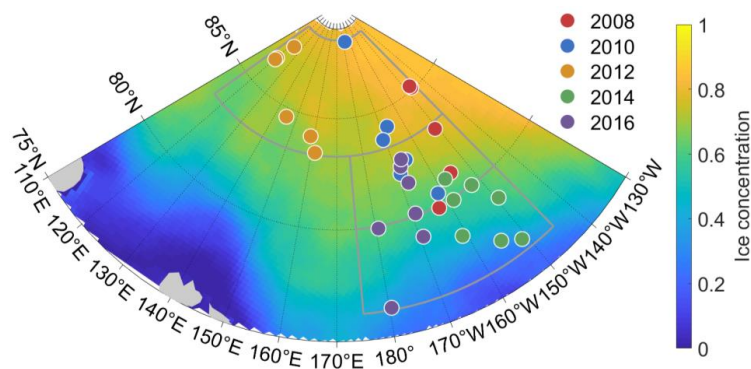
57 The Arctic sea ice cores were sampled in the Pacific sector of the Arctic Ocean during summer cruises of the CHINARE



58 program from 2008 to 2016 (Figure 1). Each ice core was evenly divided into 10 layers. Detailed volume fractions of the gas
59 bubbles and brine pockets (V_a , V_b) in the ice cores were given by Wang et al. (2020). Almost all cores were sampled in August,
60 when the ice had started to melt.

61 A typical undeformed sea ice floe consists texturally of three layers due to its growth conditions (Tucker et al., 1992). The
62 first two layers are relatively thin and consist of a granular layer and a transition layer, and the lowest layer generally consists of
63 columnar ice. The ice texture controls the ice microstructure (Crabeck et al., 2016). Thus, the development of gas bubbles,
64 brine pockets, and IOPs in the three ice layers is different. Analogous to the parameterization of the Los Alamos sea ice model
65 (CICE; Briegleb & Light, 2007), the ice was divided into ten vertical layers. The top (1/10) layer of an ice core was defined as
66 the top layer (TL), the second layer (2/10) was the drained layer (DL), and layers 4–10/10 collectively constitute the internal
67 layer (IL). Note that the surface scattering layer (SSL) and part of the DL were mixed in the TL and could not be separated
68 completely. Layer 3/10 was also a mixture of a DL and IL, and is therefore neglected in the following analysis.

69



70

71 Figure 1. Locations of the sampled ice cores during CHINARE cruises. The ice cores were assorted into three parts according to latitude
72 and ice concentration. Their quantities were nearly the same in each zone. The ice concentration in the base map was the mean in August
73 from 2008 to 2016.

74 2.2 Sea ice optics modeling

75 The IOPs of sea ice, including the scattering coefficient, σ , absorption coefficient, κ , and asymmetry parameter, g , can be
76 determined directly from the icemicrostructure. Following the theory of Grenfell (1991), scattering in ice is caused by gas
77 bubbles and brine pockets, and absorption is caused by brine pockets and pure ice. This parameterization has been proved by
78 extensive observations (e.g., Light et al., 2004; Smedley et al., 2020). The IOPs of sea ice can be obtained from the sum of the
79 scatterers weighted by their relative volumes as:



$$80 \quad \sigma = \sigma_a + \sigma_b = \int_{r_{\min}}^{r_{\max}} \pi r_a^2 Q_a^{\text{sca}} N_a(r) dr + \int_{l_{\min}}^{l_{\max}} \pi r_b^2 Q_b^{\text{sca}} N_b(l) dl \quad (1)$$

$$81 \quad \kappa = \kappa_i + \kappa_b = k_i V_i + \int_{l_{\min}}^{l_{\max}} \pi r_b^2 Q_b^{\text{abs}} N_b(l) dl \quad (2)$$

$$82 \quad g = \frac{g_a \sigma_a + g_b \sigma_b}{\sigma} \quad (3)$$

83 In these equations, the subscripts a and b represent gas bubbles and brine pockets, respectively, r is their radius (or equivalent
 84 radius), and l is the length of the brine pockets. Q^{sca} and Q^{abs} are the scattering and absorption efficiencies, respectively, which
 85 can be calculated using Mie theory. N is the size distribution function, subscript i represents pure ice, and $V_i = 1 - V_a - V_b$ is its
 86 volume fraction. The values of these parameters are summarized in Table 1. Brine pockets longer than 0.03 mm are modelled
 87 as cylinders rather than spheres (Light et al. 2003). The conversion function from Grenfell & Warren (1999) is employed to
 88 represent hexagon columns as spheres with the same optical properties. Besides, Q^{abs} and Q^{sca} in the required size range are
 89 obtained using their effective radii, which are calculated according to Hansen & Travis (1974).

90

91 Table 1. Parameters used in the radiation transfer model in Arctic summer and their sources

Parameter	Reference(s)
refractive index of gas bubbles	Light et al. (2004)
refractive index of brine pocket	Smith and Baker (1981)
N_a, N_b	Light et al. (2003)
k_i	Grenfell and Perovich (1981)
g_a, g_b	Light et al. (2004)
$r_{\min} = 0.5 \text{ mm}, r_{\max} = 2 \text{ mm}$	Grenfell (1983); Frantz et al. (2019)
$l_{\min} = 1 \text{ mm}, l_{\max} = 20 \text{ mm}$	Light et al. (2003); Frantz et al. (2019)

92

93 The Delta-Eddington multiple scattering model, where the constant IOPs from Briegleb & Light (2007) were replaced by
 94 the modeled IOPs, was employed to estimate the apparent optical properties (AOPs: albedo α_λ , transmittance T_λ , and
 95 absorptivity A_λ) of the ice at the sampling sites (Yu et al., 2022). The broadband albedo (α_B), transmittance (T_B), and
 96 absorptivity (A_B) were calculated by integrating the spectral values over band of the incident solar radiation, F_0 as:

$$97 \quad X_B = \frac{\int_{\lambda_1}^{\lambda_2} X_\lambda F_0(\lambda) d\lambda}{\int_{\lambda_1}^{\lambda_2} F_0(\lambda) d\lambda}, X = \alpha, T, A, \quad (4)$$

98 In the following sections, the broadband absorption coefficient, κ_B , was also derived by this equation, following CICE
 99 (Briegleb & Light, 2007). Considering the generally cloudy weather in Arctic summer, the incident solar irradiance under an
 100 overcast sky in August from Grenfell & Perovich (2008) was chosen as the default value for F_0 . The studied wavelength band
 101 was set as the photosynthetically active band, i.e. $\lambda_1 = 400 \text{ nm}$ and $\lambda_2 = 700 \text{ nm}$.



102 2.3 Arctic-wide up-scaling

103 To conduct an up-scaling analysis of the radiative budget of the Arctic sea ice cover based on observations of the ice
104 microstructure in the Pacific sector, we used representative basin-scale sea ice data to estimate the variations in the distribution
105 of radiation fluxes in summer during 2008-2016. The sea ice concentration (C) was provided by the National Snow and Ice
106 Data Center (NSIDC) (Cavalieri et al., 1996), the sea ice thickness was based on CryoSat-2/SMOS data fusion (Ricker et al.,
107 2017), and the incident shortwave radiation flux at the surface (E_d) was obtained from the European Centre for
108 Medium-Range Weather Forecasts (ECMWF). The latter two datasets were interpolated to a 25 km NSIDC Polar
109 Stereographic grid. Then, the mean radiation fluxes and ice concentrations from July to September from 2008 to 2016 were set
110 as the representative values in summer. Due to the limitation of satellite remote-sensing data of summer ice thickness, the
111 representative thickness was estimated according to the mean value in October from 2011 to 2016, together with the growth
112 rate estimated by Kwok and Cunningham (2016). Thus, the reflected, absorbed, and transmitted radiation flux by Arctic sea ice
113 are $E_r = E_d \cdot C \cdot \alpha_B$, $E_a = E_d \cdot C \cdot A_B$, and $E_T = E_d \cdot C \cdot T_B$, respectively.

114 3 Results

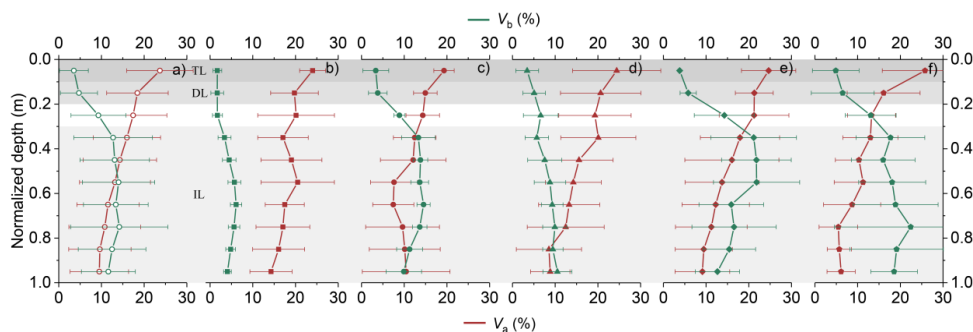
115 3.1 Microstructure of the ice cores

116 There were different variation trends in the volume fraction of gas bubbles and brine pockets (V_a , V_b) as a function of
117 ice core depth (Figure 2). The upper granular ice was typically bubbly, associated with the drainage of brines, and the interior
118 columnar ice is usually depleted in gas bubbles (Cole et al., 2004). Thus, a clear decreasing trend along depth could be seen
119 in V_a . The mean V_a of the TL, DL, and IL for all ice cores was $23.7 \pm 7.8\%$, $18.4 \pm 7.2\%$, and $12.1 \pm 7.8\%$, respectively.
120 These values are similar to the observations made by Eicken et al. (1995) where V_a decreased from $> 20\%$ at the top to $< 5\%$
121 at the bottom for summer Arctic sea ice.

122 The drainage of brine resulted in a relatively small V_b of TL, with a mean of $3.5 \pm 3.3\%$, while it was $4.7 \pm 4.3\%$ and
123 $13.1 \pm 8.4\%$ in the other two layers, respectively (Figure 2a). $V_b = 5\%$ is usually chosen as a threshold where discrete brine
124 inclusions start to connect and the columnar ice is permeable enough to enable drainage (Carnat et al., 2013). Thus, the ice
125 cores in the present study have been melting for some time, agreeing with the sampling season during CHINARE. Most V_b
126 profiles had a maximum in the middle depth, except for the ice cores in 2012 (Figure 2d). This can be explained by the later
127 sampling date in 2012 relative to the other years by about 10 days, which resulted in enhanced brine drainage. Furthermore, the
128 shape of the V_b profile was also associated with ice age (Notz and Worster, 2009). Compared with the ice cores in 2010,
129 although the ice cores in 2016 had similar sampling dates (one day difference), the maximum position of V_b in 2016 was



130 lower than in 2010 (Figure 2c, f). This was because all ice cores in 2010 were sampled from first-year ice, and the ice cores in
131 2016 were comprised of first-year ice and multiyear ice (Wang et al., 2020).



132

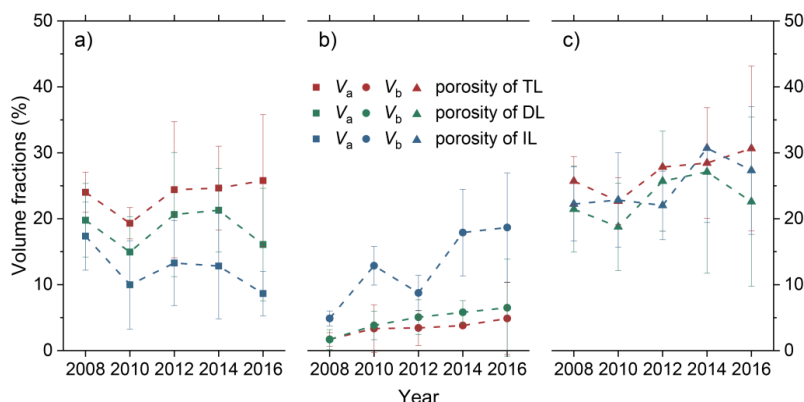
133 Figure 2. Profiles of V_a and V_b against normalized depth in (a) the whole study period, (b) 2008, (c) 2010, (d) 2012, (e) 2014, and (f) 2016.
134 The error bars showing the standard deviation from the mean of the results. The shady areas represent the ice layer structure.

135

136 In addition to the different variations in V_a and V_b with depth, the annual variations in each layer were also different
137 (Figure 3a). V_a was relatively small in the TL of 2010 because all ice cores were sampled from first-year ice (Wang et al., 2020).
138 While the quantities of first-year ice cores were similar to the amount of multiyear ice cores in the other years, the overall
139 trends were still clear. Compared with 2008, the V_a of TL in 2016 increased by 7.5%. This indicated that the melting process of
140 the ice surfaces of the cores in 2016 was more dramatic than in 2008. Contrary to the TL, the V_a in the IL tended to decrease
141 from 2008 to 2016. The corresponding variation ratio was -50.3%. The V_a values of DL were relatively stable, which did not
142 show a clear increase or decrease in the study period.

143 Things were different for V_b and ice porosity. There were clear increases in the V_b of all three ice layers (Figure 3b),
144 which implied dramatic variations in the permeability of summer sea ice. Furthermore, increases of V_b in the DL and IL were
145 clearer than in the TL. From 2008 to 2016, the increase in the IL was clearest. Meanwhile, the increases in V_b of the TL and
146 DL were similar. Simultaneously, the ice salinity of the IL decreased (Figure S1), which agreed well with the observed and
147 modeled results with warming conditions (e.g., Vancoppenolle et al., 2009). From the combined effects of changing V_a and
148 V_b , it was clear that the porosity of ice was on the increase (Figure 3c). Furthermore, no obvious differences in the
149 developments of porosity were seen in the three layers.

150



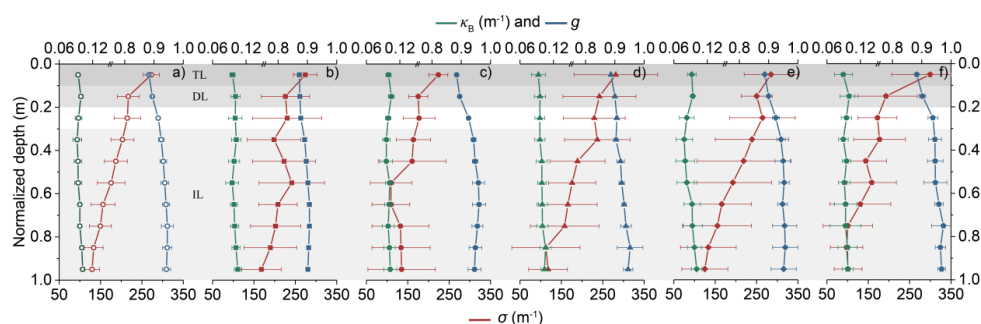
151

152 Figure 3. Variations in (a) V_a , (b) V_b , and (c) the porosity of the TL, DL, and IL of the ice cores during 2008 to 2016.

153 **3.2 Variations in the IOPs of the ice cores**

154 The mean scattering coefficient, σ , of the TL, DL, and IL for all ice cores was $272.8 \pm 25.8 \text{ m}^{-1}$, $217.3 \pm 28.7 \text{ m}^{-1}$, and
 155 $162.0 \pm 27.4 \text{ m}^{-1}$, respectively (Figure 4a). There was a clear decreasing tendency along with depth in the mean σ of all ice
 156 cores, associated with a decreasing volume of gas bubbles (Figure 2). Although the V_b values of the ice cores increased clearly
 157 with depth, they did not enhance the scattering capacity of ice. The reason for this was that the refractive indices of brine
 158 pockets and pure ice are close (Smith and Baker, 1981; Grenfell and Perovich, 1981).

159 The vertical variations in κ_B and g were not clear as seen for σ because they depend on V_i and V_b/V_a , respectively. Due to
 160 the low porosity of the ice ($V_a + V_b$), κ_B showed a slightly increasing trend with depth, which varied in the range $0.09\text{--}0.1 \text{ m}^{-1}$.
 161 The mean value of g was 0.93 except in 2008 (which was $g = 0.89$), and it slightly increase with depth. This value is smaller
 162 than the commonly used one; for example, the previous typical range of g was from 0.86 to 0.99 (e.g., Ehn et al., 2008), and
 163 0.94 was often adopted for computational efficiency in models (Light et al., 2008). However, we note that particulate matter
 164 and inclusion shape were not considered here, which may be a possible reason for the different values of g found here.



165

166 Figure 4. IOP profiles of ice cores against normalized depth in (a) the whole study period, (b) 2008, (c) 2010, (d) 2012, (e) 2014, and (f)



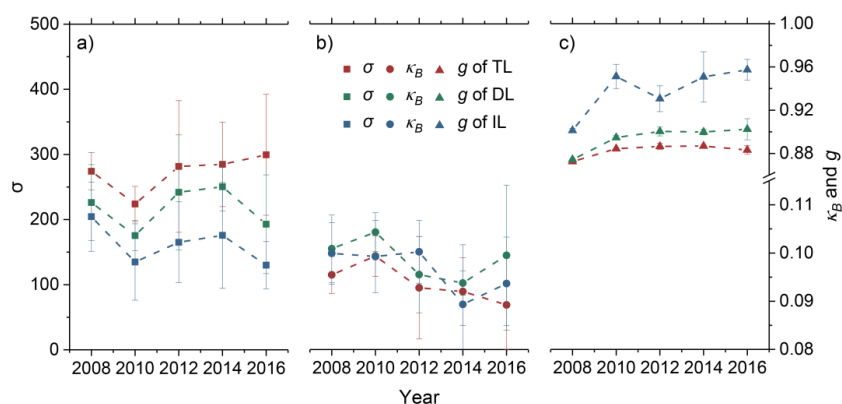
167 2016.

168

169 The annual IOPs of the TL, DL, and IL of the ice cores are shown in Figure 5. As shown in Figure 5a, the variations in σ of
 170 the TL, DL, and IL were different. A generally increasing σ could be identified in the TL. Compared with 2008, the σ of the TL
 171 in 2016 increased by 9.3% due to the increased V_a of the ice. A similar phenomenon was observed by Light et al. (2008), where
 172 the σ of the ice surface layer increased as melting progressed. The variations of the σ for the DL were not as clear as for the TL
 173 due to ongoing drainage. Overall variations in the σ of the IL were contrary to those seen for the TL. Compared with 2008, the
 174 σ of the IL in 2016 decreased by 36.4% due to the decreased V_a (Figure 3).

175 The broadband absorption coefficient, κ_B , of the TL and IL in 2016 decreased by about 6% relative to their values in 2008
 176 (Figure 5b). Similar variations were not clear in the κ_B values of the DL. Because the absorption in sea ice is mainly caused by
 177 pure ice and brine pockets, the absorption efficiency is weaker in brine than in pure ice; thus, an increasing porosity results in
 178 decreasing κ_B . As shown in Figure 5c, the values of g of the TL and DL were nearly constant. Because their values of V_b were
 179 sufficiently small due to drainage (Figure 3b), their values of g are mainly attributed to gas bubbles. In contrast, the values of g
 180 of the IL increased by 5% with increasing V_b in the study years (Figure 3b).

181



182

183 Figure 5. Annual (a) σ , (b) κ_B , and (c) g for the TL, DL, and IL of the ice cores from 2008 to 2016.

184

185 3.3 Variations in the AOPs of the ice cores

186 Having seen that the IOPs of the sea ice were not constant in the different years (Figure 5), a more important question is
 187 how these changes affected the AOPs. The AOPs of the sampling sites are shown in Figure 6. Note that the AOPs here were



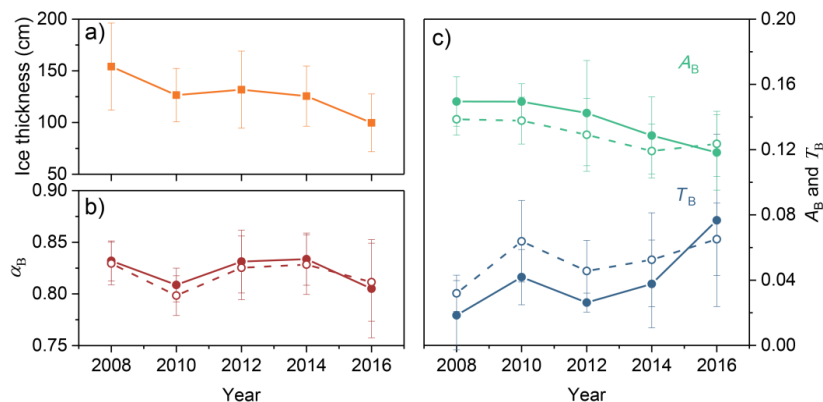
188 based on level ice. Surface properties, such as a snow layer or melt ponds, were not considered here, because the focus was on
189 the effects of the ice microstructure on their AOPs. The results obtained with the same IOPs profiles but for a constant ice
190 thickness (1 m) are also presented to quantify the contributions from the ice microstructure and thickness separately.

191 The values of α_B changed because of the effects of the ice IOPs and thickness (Figure 6b). The variations in α_B were
192 similar to those in the σ of the TL and DL; i.e., the IOPs of the upper-most ice largely controlled the albedo of bare ice, which
193 was also observed in field observations (e.g., Light et al., 2015). Besides, the α_B values did not present clear decreases. This
194 was different from the remote-sensing results (-0.05 per decade for 1982 to 2009) of Lei et al. (2016). The reason for this was
195 the direct factor that reduces the annual ice albedo is not the ice microstructure but rather the surface conditions. Eicken et al.
196 (2004) and Landy et al. (2015) reported that the evolution of melt ponds on the ice surface could explain 85% of the variance in
197 the summer ice albedo.

198 Different from α_B , T_B (A_B) tended to increase (decrease) clearly (Figure 6c). The value of T_B in 2016 was over treble of
199 that in 2008. Meanwhile, A_B decreased by about 20.9% from 2008 to 2016. Furthermore, the change of A_B in the study years
200 was lower than the actual change in the ice thickness (-35.3%). Thus the difference, 22.3% ($\frac{1-20.9\%}{1-35.3\%} - 1$), was attributed to an
201 increase in the absorbed solar energy per unit volume of sea ice. The increasing absorbed radiation due to the changing IOPs
202 and thickness of the ice may enhance internal melting.

203 To make a direct comparison with the above variations, we considered a constant ice thickness, finding that the changes in
204 the AOPs were different but the overall trends were similar (dashed lines in Figure 6). T_B increased from 0.03 to 0.06 from
205 2008 to 2016, accounting for about 32.9% of the real change with changing thickness. Thus, the changing microstructure of the
206 melting ice resulted in an increased transmittance that was independent of the ice thickness. A similar result was observed in
207 the laboratory, where the changing ice microstructure during the warming process (no decrease in thickness) increased the ice
208 transmittance (Light et al., 2004). Different from T_B , whether the thickness was taken into account or not, the overall trends in
209 α_B and A_B were hardly affected. This demonstrated that the present variations in ice thickness had more effects on the ice T_B
210 than α_B and A_B .

211



212

213 Figure 6. (a) Thickness and (b, c) estimated AOPs of the ice cores from 2008 to 2016. Also shown as dashed lines are the AOPs with the
 214 same IOPs and constant thickness (1 m).

215 3.4 Arctic-wide analysis

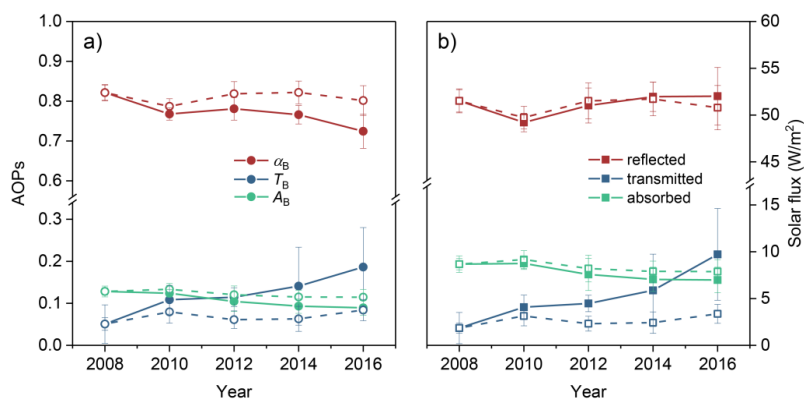
216 In this section, we expand the variations of the ice cores (Figure 5) to an Arctic-wide scale under the following
 217 assumptions. First, the IOPs of Arctic ice were based on the results derived from the ice cores. This follows the common
 218 approach used in current models, i.e. they are taken as constant and seasonal and spatial differences are ignored (e.g., Briegleb
 219 and Light, 2007). Second, a decreasing trend of -5.8 cm yr^{-1} in ice thickness according to Lindsay and Schweiger (2015) was
 220 adopted to get a general view of the contributions of the changing ice thickness on the radiation budget. The representative
 221 basin-scale sea ice and radiation data in summer were used here to estimate the variations in the distribution of radiation fluxes.

222 With the combined effects of the changing microstructure and thickness of ice, Arctic-wide variations in the mean α_B , T_B ,
 223 and A_B (Figure 7a) were clearer than those in Figure 6, especially the overall trends of the mean T_B ($r = 0.97$, $p < 0.01$) and A_B
 224 ($r = -0.97$, $p < 0.01$) of ice. Although the mean α_B decreased during 2008 to 2016, there was not much change in E_r , only about
 225 51.1 W m^{-2} during the study years (Figure 7b). This was because the decreasing α_B was largely provided by marginal ice zones.
 226 The decreasing rate of α_B in regions with ice thicknesses $< 1 \text{ m}$ (equivalent to 16.4% of the entire ice area) was over 1.6 times
 227 the rate of the entire ice cover (Figure S2). With the retreat of sea ice, the reflected flux of the marginal zone contributes less
 228 and less to the reflected flux of the entire ice cover.

229 The mean transmitted solar radiation, E_T , increased from 1.8 W m^{-2} to 9.7 W m^{-2} from 2008 to 2016 (Figure 7b). Most of
 230 the increase in E_T is ascribed to thin ice in marginal ice zones (ice thicknesses $< 1 \text{ m}$), which contributed 49.2% of the
 231 increasing E_T from 2008 to 2016 (Figure 8a–e). Meanwhile, E_a decreased from 15 W m^{-2} in 2008 to 13.8 W m^{-2} in 2016. As the
 232 decrease in ice volume from 2008 to 2016 was 32.2%, the solar energy absorbed by a unit volume of sea ice increased by 35.7%
 233 on the Arctic scale.



234



235

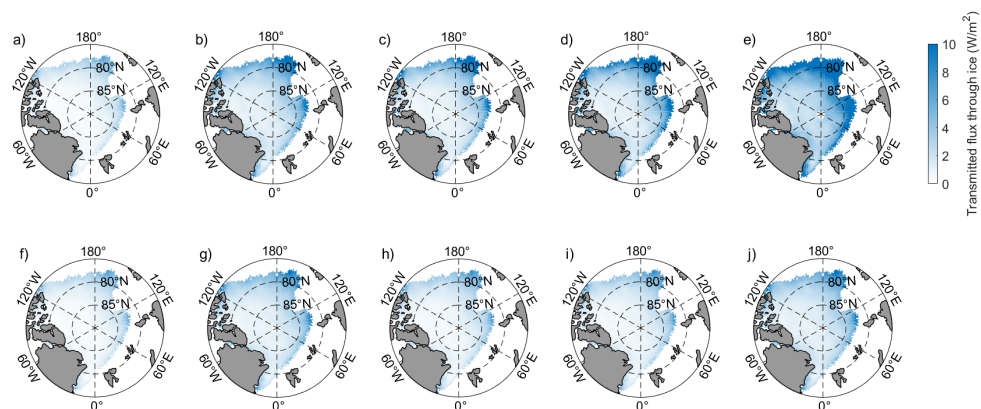
236 Figure 7. Arctic-wide variations in the mean (a) AOPs of ice and (b) solar flux distribution during 2008 to 2016. Also shown as dashed
237 lines are the AOPs and fluxes with the same IOPs and constant thickness field.

238

239 When the ice thickness was set as a constant, variations in the mean AOPs were different, which resulted in differences
240 in the solar flux (dashed lines in Figure 7b). Among them, differences in the reflected flux were relatively small. Meanwhile,
241 the mean E_T increased from 1.8 W m^{-2} in 2008 to 3.4 W m^{-2} in 2016. E_a decreased from 8.7 W m^{-2} to 7.9 W m^{-2} in the same
242 period. These changes corresponded to 19.3% and 46.8% of the combined effects of the ice IOPs and thickness, respectively,
243 from 2008 to 2016. Furthermore, marginal ice zones with ice thicknesses $< 1 \text{ m}$ still contributed 37.1% of the increasing E_T
244 from 2008 to 2016 (Figure 8f-j). This value was about 75.4% of the rate of the combined effects of the changing IOPs and
245 thickness of ice. In other words, the same changes in the ice microstructure had more effects on the T_B of thin sea ice, and these
246 effects were clearer than those resulting from general decreasing ice thickness.



247



248

249

250 Figure 8. Distribution of transmitted solar radiation through sea ice in the summers of 2008 to 2016 when the sea ice thickness was set (a–e)
251 to decrease and (f–j) to a constant value. Only flux that penetrated through the sea ice is considered in this map.

252 4 Discussion

253 4.1 Comparisons with IOP measurements

254 In Section 3.2, we estimated the ice IOPs according to the observed ice physics and structural-optical theory. Other
255 methods estimated ice IOPs in previous studies. In this section, we compared the ice scattering coefficient, the most variable
256 value among all IOPs, determined in the present study with previous results (Figure 9). The differences in wavelength bands
257 were ignored in the comparisons because σ was nearly wavelength-independent.

258 It is clear from Figure 9 that the range of σ of the present study covered the majority of previous results. The derived
259 values of σ for the SSL and DL of melting bare ice in August ranged from 920 to 2,000 m^{-1} and 40 to 150 m^{-1} , respectively
260 (Light et al., 2008). According to the layer structure, wherein the TL was composed of a 5 cm SSL and the others were DLs, the
261 bulk σ of the TL in Light et al. (2008) ranged from 270 to 435 m^{-1} . This result was slightly higher than our results. The results
262 of Mobley et al. (1998) and Perron et al. (2021) agree with our range. The σ of the DL in Perron et al. (2021) was in our range,
263 and the values of Light et al. (2008) were smaller than those in the present study.

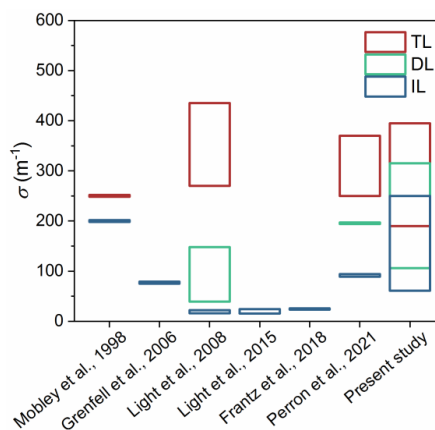
264 Differences in the σ of the IL were clearer than in the TL and DL. The σ values of the IL of most our cores were relatively
265 larger than those of Light et al. (2008, 2015) and Frantz et al (2019). In these results, Light et al. (2008) estimated the σ using
266 the observed ice albedo and a three-layer structure with fixed thicknesses. The results of Light et al. (2015) and Frantz et al.
267 (2019) were obtained in a cold laboratory by simulating the radiative transport in subsections of the sea ice. Meanwhile, the
268 results of Grenfell et al. (2006) and Perron et al. (2021) are close to the minimum of our range. The σ of ice in Grenfell et al.,
269 (2006) was calculated from the ice extinction coefficient, and it was measured *in situ* using a diffuse reflectance probe in the



270 Perron et al. (2021). The values calculated by the same method as used in the present study by Mobley et al. (1998) were
271 close to the maximum of our range. Thus, it was expected that the differences in the IL's σ largely resulted from the different
272 methods used in the myriad studies.

273 One possible reason for the differences was the uncertainties in the ice microstructure introduced by brine loss during
274 measurement and segmenting. Thus, our V_a values of the IL are greater than the values derived from nondestructive methods
275 (e.g., Perron et al., 2021). As a result, the maximum underestimate of V_b was 15–25% and the maximum overestimate of V_a was
276 96–160% when taking the uncertainties introduced by the measurements and brine drainage into account (Wang et al., 2020).
277 Taking the mean V_a and V_b of all ice cores as an example, these uncertainties overestimated the σ of the IL by 78 m^{-1} at most.
278 Although brine loss during sampling and measurements introduced uncertainties to V_a and V_b , the methods used for obtaining
279 and measuring the ice cores during the CHINARE cruises were the same. Therefore, the uncertainties introduced by the
280 methodology hardly affected the changes seen in Figure 6 and Figure 7.

281



282

283 Figure 9. Comparison of the ice scattering coefficient in the present study to the published results for Arctic sea ice using various methods.
284 All comparison results have been scaled to the layer structure used in the current study according to their ice thicknesses.

285

286 Another source of difference is the distribution function of gas bubbles employed in the IOP parameterization. Many
287 distributions are obtained in a cold laboratory, where the ice temperature is not consistent with that in the summer Arctic. As
288 the refractive indices of brines and pure ice were similar, the distribution function of brine pockets had a smaller influence on
289 the ice IOPs than gas bubbles (Yu et al., 2022). Here, we tentatively adjusted the exponent of the distribution function of the
290 gas bubbles from its default value of -1.5 to -1, i.e., the fraction of small bubbles decreases, which coincides with warming ice



291 (Light et al., 2003). Then, the changed distribution function was used for 1 m thick ice with mean values of V_a and V_b for every
292 ice core. This change resulted in an uncertainty of 8 m^{-1} in the σ of each layer. These uncertainties did not alter the above results
293 and are considered acceptable.

294 Although brine loss and the difference in the distribution functions of gas bubbles introduced uncertainties in σ , they did
295 not affect the ice AOPs much. Considering a 1 m thick ice layer described by the mean physics of ice cores, the effects of the
296 former factor on the ice AOPs were less than 0.02. The uncertainties in α_B and T_B introduced by the latter factor were 0.005 and
297 0.002, respectively. Therefore, our estimated α_B range (0.76–0.87) agreed with the observed results of Light et al. (2008, 2015)
298 and Grenfell et al. (2006). Meanwhile, the estimated T_B (0.01–0.1) was also in the corresponding observed ranges.

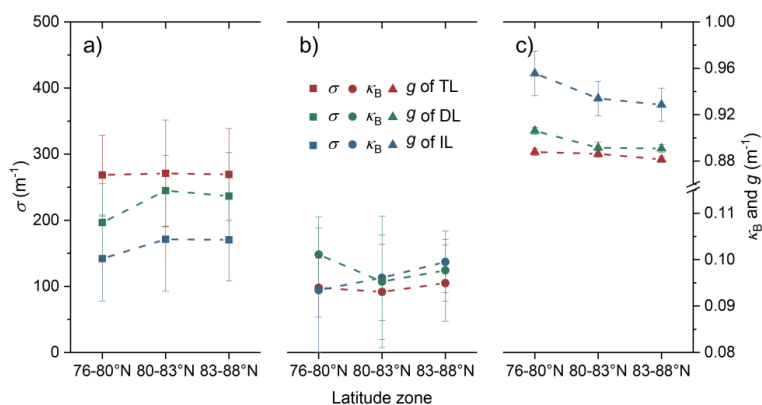
299 **4.2 On the interannual variations of the IOPs**

300 Extensive measurements of the IOPs of Arctic sea ice have been carried out, and some authors have noticed the seasonal
301 variations of the ice microstructure and IOPs (e.g., Light et al., 2008; Frantz et al., 2019; Katlein et al., 2021). However,
302 interannual variations in sea ice IOPs are still not clear, although such changes in sea ice extent, thickness, and age are evident.
303 A lack of continuous IOP measurements is the primary reason. Compared with previous observations, the ice core data in the
304 present study were more appropriate for interannual analyses of the IOPs of ice because of their long time span and
305 consistencies in the sampling method, seasons, and sea areas. The reasons we could not introduce other ice core data (SHEBA,
306 ICESCAPE, N-ICE, MOSAiC, etc.) into this study was that not only the differences in sampling seasons, sites, and methods
307 increase the dispersion in time and space during such an analysis, but also the lack of information about the ice
308 microstructure or essential physical properties will limit how much we can determine from such a comparison. Considering
309 that sampling ice cores is a commonly used method for *in situ* observations, with more suitable ice core data in the future,
310 large-scale time series of ice IOPs may be obtained.

311 The ice cores used in the present study were sampled at different ice stations but not at the same floe (Figure 1). Thus, the
312 data did not form a time series in the strictest meaning. Figure 10 illustrates the different IOPs of the ice cores in three latitude
313 zones, which shows that there are spatial differences in the present ice core data. Among the three IOPs, variations in σ are the
314 clearest. The difference in κ_B and g in the different latitude zones were not more than 5% and 2%, respectively (Figure 10b,
315 c). As a transition layer between the TL and IL, variations in the IOPs of the DL were more discrete than in the other two
316 layers. For σ , there were no clear changes in the TL. This demonstrated that the variations of σ in the TL largely resulted
317 from interannual factors. Meanwhile, the differences in the σ of the IL are clear. With an increase of latitude, the σ of the IL
318 tended to increase. The rate of spatial variation of σ in the IL can be up to 16.5% in the different latitude zones. This value
319 was equivalent to 45.8% of the maximum rate of interannual variation seen in Figure 5.



320



321

322 Figure 10. Different values of (a) σ , (b) κ_B , and (c) g for the TL, DL, and IL of the ice cores in the three latitude zones.

323

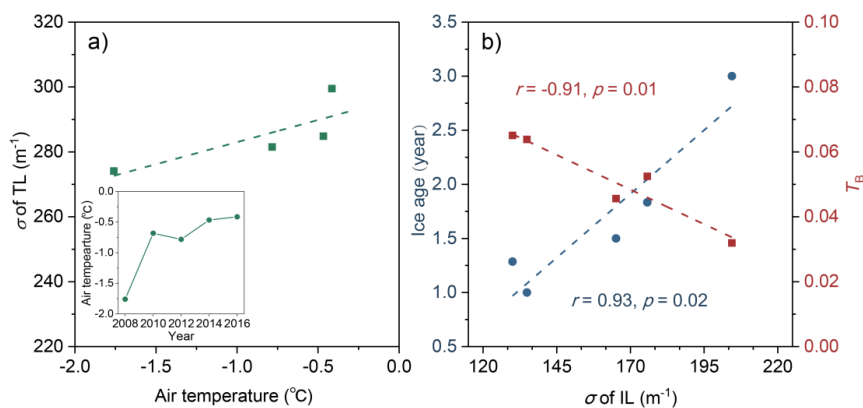
324 The melting days of sampling sites, which were calculated according to the sampling date ($Aug. 18 \pm 9$ days) and melt
 325 onset from Markus et al. (2009), were similar (58 ± 7 days). The amount of surface radiation during the study years was also
 326 similar (Laliberté et al., 2021). However, the observed air temperature increased continuously (Figure 11a). This clear
 327 difference in the temperatures of the sampling date can hardly be explained by spatial variations, but agree more with the
 328 interannual variations (e.g., Collow et al., 2020). Previous observations demonstrated that the evolution of the σ of the SSL is
 329 highly affected by warming processes (e.g., Light et al., 2008; Smith et al., 2022). Except for the ice cores in 2010, the
 330 variations in the σ of the TL in the present study agreed with the increasing air temperature (Figure 11a).

331 There were clear differences in the σ of the IL (Figure 5a) which can hardly be explained by increasing air temperature
 332 because the σ of the IL is relatively constant (Light et al., 2008) and even increases in the melt season (Frantz et al., 2019).
 333 Figure 11b shows the correlations among the annual σ of the IL, ice age, and T_B . Note that T_B here is the result under the
 334 assumption of a constant ice thickness (dashed line in Figure 6c). The ice ages were obtained according to fieldwork (Wang et
 335 al., 2020) and remote-sensing data (Tschudi et al., 2019). Because the ice age of each grid cell in the remote-sensing data is
 336 represented as the age of the oldest floe, once an ice core was distinguished as first-year ice in the fieldwork, the corresponding
 337 ice age was set as one year regardless of the remote-sensing data. The use of remote-sensing data is acceptable because the ice
 338 cores in this study were all sampled in large and thick floes for safe fieldwork. These floes were more likely older than the
 339 surrounding ice. Figure 11b demonstrates that the decrease in the σ of the IL is correlated with decreasing ice age. The σ of the
 340 IL in the first-year ice was smaller than in multiyear ice, which was also observed by Light et al. (2015). This could partly
 341 explain the spatial variations in the σ of the IL (Figure 10a) because ice in high latitude zones was likely older than in the other



342 zones (Stroeve and Notz, 2018).

343



344

345 Figure 11. (a) Changing air temperature at the sampling sites and its effects on the σ of the TL. (b) Correlations among the σ of the IL with
346 ice age and T_B .

347

348 In summary, the differences in the IOPs of the ice cores were related to interannual variations in the air temperature and
349 ice age. The changing ice age largely manifested in the ice microstructure in the IL. In other words, the changing ice age may
350 be partly responsible for the modeled results shown in Figure 7, even without any decrease in the ice thickness. To our
351 knowledge, this is the first study to link ice microstructure and IOPs at interannual scales. Although these ice core data are not
352 a time series in the strictest meaning, they are still helpful for understanding the general effects of the scenario where the Arctic
353 is warming and the ice ages are decreasing. Our results suggested that in this scenario, the σ values of the TL and IL of summer
354 ice tended to be greater and smaller than before, respectively. It is expected leading to interannual trends of the ice
355 microstructure and IOPs. This process needs to be confirmed by future observations and more simulations.

356 4.3 Implications for the future Arctic

357 Previous studies have reported that surface properties (snow, ponds, etc.) largely control the variations in the ice albedo
358 (Landy et al., 2015). The present results also asserted that interannual variations in the ice's microstructure or IOPs had little
359 effect on the albedo of bare ice (< 2%), but they do play an important role in ice transmittance (Figure 6). With continued
360 Arctic warming, the summer ice age is on the decrease, and the ice microstructure and IOPs change accordingly, leading to an
361 overall higher ice transmittance. Furthermore, the transmitted solar energy affects the temperature of the upper ocean and
362 results in further melting of the bottom of sea ice (Timmermans, 2015). Along with the melting of ice, gas bubbles and brine



363 pockets change simultaneously (Light et al., 2004), which affect the IOPs of ice in turn. Consequently, the sea ice is expected to
364 become thinner and more porous than before. This process has been seldom considered in previous studies. Related studies
365 generally regarded the surface properties and thickness of the ice as predictors for light transmittance (e.g., Katlein et al., 2015;
366 Perovich et al., 2020). The microstructure and morphological parameters of sea ice (e.g., thickness, extent, etc.) may together
367 influence the melting processes of Arctic sea ice.

368 For safe field observations, the ice core data used in this study were all sampled in large and thick floes. Variations in the
369 microstructure of the ice in marginal zones or under melt ponds cannot be addressed by this study. Light et al. (2015) reported
370 that the differences in the σ between the IL of ponded first-year ice and multiyear ice were larger than the those between bare
371 first-year ice and multiyear ice. The changes in the IOPs of the marginal ice zone were expected to be more obvious than found
372 in the present results because ice in marginal zones is more likely young and ponded (Rigor and Wallace, 2004; Zhang et al.,
373 2018). Furthermore, the same changes in the ice microstructure have more effects on the T_B of thin sea ice (Section 3.4).
374 Marginal ice zones, comprising 16.4% of the entire ice area, contributed 37.1% of the extra-transmitted solar energy due to the
375 ice changing microstructure from 2008 to 2016 (Figure 8). Both processes promote an increase of transmitted flux through sea
376 ice and ice bottom melting in marginal ice zones. Arndt & Nicolaus (2014) quantified light transmittance through sea ice into
377 the ocean for all seasons as a function of variable sea ice types. The mean annual trend was 1.5% per year, which mainly
378 depended on the timing of melt onset. If the variations in the microstructure of bare and ponded ice are taken into consideration,
379 this trend is expected to increase. We suggest that future ice observations and models should pay more attention to variations
380 in the ice age, microstructure, and their effects, especially in marginal ice zones.

381 5 Conclusions

382 Based on ice cores sampled during the CHINARE expeditions (2008–2016), interannual variations in the IOPs of Arctic
383 sea ice in summer due to the changing microstructure of ice were modeled according to structural-optical theory. Variations in
384 the AOPs and solar flux distribution due to the changing IOPs in the summer Arctic were also estimated. Clear variations in the
385 microstructure and IOPs of each year (Figure 5) enabled us to construct a quantitative view of changes that the Arctic sea ice
386 interior underwent in these years.

387 As a result of our study, it was found that interannual variations in V_a , V_b , and the IOPs of three ice layers were different,
388 and the overall trends of V_a in TL and IL were nearly the opposite. Meanwhile, increases in V_b could be seen in each layer,
389 and the increase in IL was the clearest. These changes in microstructure were related to the increasing air temperature and
390 decreasing ice ages. The ice σ were highly affected by V_a , which results in the different interannual changes in the σ of the



391 different layers. The bare ice albedo was mainly controlled by the σ of the upper layers (TL and DL), and the transmittance is
392 highly correlated with the σ of the IL. With the combined effects of changing microstructure in each ice layer, the interannual
393 variations in the transmitted radiation through the ice were clearer than in the albedo of bare ice, especially in marginal ice
394 zones (Figure 8).

395 Previous studies paid more attention to changing transmittance due to declining ice thickness. The present findings
396 demonstrated that the changing IOPs derived from the ice microstructure could also alter the partitioning of solar radiation in
397 sea ice by itself. With continued Arctic warming, summer ice will become younger and more porous than before, leading to
398 more light reaching the upper ocean. This reminds us to pay more attention to the variations in the IOPs of interior ice,
399 especially ice with different ages.

400

401 *Acknowledgments.* We are grateful to the NSIDC, Alfred Wegener Institute, and ECMWF for providing the sea ice and
402 radiation data. This work was financially supported by the National Key Research and Development Program of China (Grant
403 number 2018YFA0605901), the National Natural Science Foundation of China (Grant numbers 41922045, 41906198,
404 41976219, and 41876213), and the Academy of Finland (Grant numbers 333889, 325363, and 317999). We also wish to
405 acknowledge the crews of the R/V Xuelong for their fieldwork during CHINARE.

406 *Author contributions.* MY carried out the estimations and wrote the paper. RL, BL, and QW provided the ice core data. All
407 coauthors discussed the results and edited the manuscript.

408 *Data Availability Statement.* The sea ice and radiation data are available at <https://nsidc.org/data>;
409 [https://data.meereisportal.de/gallery/index_new.php?lang=en_US&ice-type=extent&active-tab1=measurement&active-tab2=](https://data.meereisportal.de/gallery/index_new.php?lang=en_US&ice-type=extent&active-tab1=measurement&active-tab2=thickness)
410 [thickness](https://data.meereisportal.de/gallery/index_new.php?lang=en_US&ice-type=extent&active-tab1=measurement&active-tab2=thickness); <https://cds.climate.copernicus.eu/cdsapp#!/home>. The ice cores data applied in this work can be accessed by the link:
411 <https://doi.org/10.5281/zenodo.6693981>.

412 *Competing interests.* The authors declare that they have no conflict of interest

413

414 **References:**

- 415 Arndt, S. and Nicolaus, M., 2014. Seasonal cycle and long-term trend of solar energy fluxes through Arctic sea ice. The
416 Cryosphere, 8 (6): 2219-2233. doi:10.5194/tc-8-2219-2014
- 417 Briegleb, B. P. and Light, B., 2007. A Delta-Eddington Multiple Scattering Parameterization for Solar Radiation in the Sea
418 Ice Component of the Community Climate System Model (No. NCAR/TN-472+STR). University Corporation for
419 Atmospheric Research. doi:10.5065/D6B27S71
- 420 Carnat, G. and Papakyriakou, T., et al., 2013. Investigations on physical and textural properties of Arctic first-year sea ice in
421 the Amundsen Gulf, Canada, November 2007–June 2008 (IPY-CFL system study). Journal of Glaciology, 59 (217):



- 422 819-837. doi:10.3189/2013JoG12J148
- 423 Cavalieri, D. J. and Parkinson, C. L., et al., 1996. updated yearly. Sea Ice Concentrations from Nimbus-7 SMMR and DMSP
424 SSM/I-SSMIS Passive Microwave Data, Version 1. Boulder, Colorado USA. NASA National Snow and Ice Data
425 Center Distributed Active Archive Center.. doi:https://doi.org/10.5067/8GQ8LZQVL0VL
- 426 Cole, D. M. and Eicken, H., et al., 2004. Observations of banding in first-year Arctic sea ice. *Journal of Geophysical*
427 *Research: Oceans*, 109 (C8): n/a-n/a. doi:10.1029/2003JC001993
- 428 Collow, A. B. and Cullather, R. I., et al., 2020. Recent Arctic Ocean Surface Air Temperatures in Atmospheric Reanalyses
429 and Numerical Simulations. *Journal of Climate*, 33 (10): 4347-4367. doi:10.1175/JCLI-D-19-0703.1
- 430 Comiso, J. C. and Parkinson, C. L., et al., 2008. Accelerated decline in the Arctic sea ice cover. *Geophysical Research*
431 *Letters*, 35 (1): L01703. doi:10.1029/2007GL031972
- 432 Crabeck, O. and Galley, R. J., et al., 2019. Evidence of Freezing Pressure in Sea Ice Discrete Brine Inclusions and Its Impact
433 on Aqueous - Gaseous Equilibrium. *Journal of Geophysical Research: Oceans*, 124 (3): 1660-1678.
434 doi:10.1029/2018JC014597
- 435 Crabeck, O. and Galley, R., et al., 2016. Imaging air volume fraction in sea ice using non-destructive X-ray tomography. *The*
436 *Cryosphere*, 10 (3): 1125-1145. doi:10.5194/tc-10-1125-2016
- 437 Dai, A. and Luo, D., et al., 2019. Arctic amplification is caused by sea-ice loss under increasing CO₂. *Nature*
438 *Communications*, 10 (1). doi:10.1038/s41467-018-07954-9
- 439 Ehn, J. K. and Papakyriakou, T. N., et al., 2008. Inference of optical properties from radiation profiles within melting
440 landfast sea ice. *Journal of Geophysical Research*, 113: C09024. doi:10.1029/2007JC004656
- 441 Eicken, H. and Grenfell, T. C., et al., 2004. Hydraulic controls of summer Arctic pack ice albedo. *Journal of Geophysical*
442 *Research: Oceans*, 109 (C08007): n/a-n/a. doi:10.1029/2003JC001989
- 443 Eicken, H. and Lensu, M., et al., 1995. Thickness, structure, and properties of level summer multiyear ice in the Eurasian
444 sector of the Arctic Ocean. *Journal of Geophysical Research*, 100 (C11): 22697-22710. doi:10.1029/95JC02188
- 445 Frantz, C. M. and Light, B., et al., 2019. Physical and optical characteristics of heavily melted "rotten" Arctic sea ice. *The*
446 *Cryosphere*, 13 (3): 775-793. doi:10.5194/tc-2018-141
- 447 Frantz, C. M. and Light, B., et al., 2019. Physical and optical characteristics of heavily melted "rotten" Arctic sea ice. *The*
448 *Cryosphere*, 13 (3): 775-793. doi:10.5194/tc-13-775-2019
- 449 Grenfell, T. C., 1983. A theoretical model of the optical properties of sea ice in the visible and near infrared. *Journal of*
450 *Geophysical Research: Oceans*, 88 (C14): 9723-9735. doi:10.1029/JC088iC14p09723
- 451 Grenfell, T. C., 1991. A radiative transfer model for sea ice with vertical structure variations. *Journal of Geophysical*
452 *Research: Oceans*, 96 (C9): 16991-17001. doi:10.1029/91JC01595
- 453 Grenfell, T. C. and Light, B., et al., 2006. Spectral transmission and implications for the partitioning of shortwave radiation
454 in arctic sea ice. *Annals of glaciology*, 44 (1): 1-6. doi:10.3189/172756406781811763
- 455 Grenfell, T. C. and Perovich, D. K., 1981. Radiation Absorption Coefficients of Polycrystalline ice from 400 to 1400 nm.
456 *Journal of Geophysical Research*, 86 (C8): 7447-7450. doi:10.1029/2007JD009744
- 457 Grenfell, T. C. and Perovich, D. K., 2008. Incident spectral irradiance in the Arctic Basin during the summer and fall.
458 *Journal of Geophysical Research*, 113: D12117. doi:10.1029/2007JD009418
- 459 Grenfell, T. C. and Warren, S. G., 1999. Representation of a nonspherical ice particle by a collection of independent spheres
460 for scattering and absorption of radiation. *Journal of Geophysical Research*, 104 (D24): 31697-31709.
461 doi:10.1029/1999JD900496
- 462 Hansen, J. E. and Travis, L. D., 1974. Light scattering in planetary atmosphere. *Space Science Reviews*, 16: 527-610.
463 doi:10.1007/BF00168069
- 464 Hunke, E. C. and Notz, D., et al., 2011. The multiphase physics of sea ice: a review for model developers. *The Cryosphere*, 5
465 (4): 989-1009. doi:10.5194/tc-5-989-2011
- 466 Katlein, C. and Arndt, S., et al., 2015. Influence of ice thickness and surface properties on light transmission through Arctic



- 467 sea ice. *Journal of Geophysical Research: Oceans*, 120 (9): 5932-5944. doi:10.1002/2015JC010914
- 468 Katlein, C. and Arndt, S., et al., 2019. Seasonal Evolution of Light Transmission Distributions Through Arctic Sea Ice.
469 *Journal of Geophysical Research: Oceans*, 124 (8): 5418-5435. doi:10.1029/2018JC014833
- 470 Katlein, C. and Valcic, L., et al., 2021. New insights into radiative transfer within sea ice derived from autonomous optical
471 propagation measurements. *The Cryosphere*, 15 (1): 183-198. doi:10.5194/tc-15-183-2021
- 472 Kwok, R., 2018. Arctic sea ice thickness, volume, and multiyear ice coverage: losses and coupled variability (1958-2018).
473 *Environmental research letters*, 13 (10): 105005. doi:10.1088/1748-9326/aae3ec
- 474 Kwok, R. and Cunningham, G. F., 2016. Contributions of growth and deformation to monthly variability in sea ice thickness
475 north of the coasts of Greenland and the Canadian Arctic Archipelago. *Geophysical Research Letters*, 43 (15):
476 8097-8105. doi:10.1002/2016GL069333
- 477 Laliberté, J. and Bélanger, S., et al., 2021. Seasonal and interannual variations in the propagation of photosynthetically
478 available radiation through the Arctic atmosphere. *Elementa: Science of the Anthropocene*, 9 (1).
479 doi:10.1525/elementa.2020.00083
- 480 Landy, J. C. and Ehn, J. K., et al., 2015. Albedo feedback enhanced by smoother Arctic sea ice. *Geophysical Research*
481 *Letters*, 42 (24): 10,714-10,720. doi:10.1002/2015GL066712
- 482 Lei, R. and Tian-Kunze, X., et al., 2016. Changes in summer sea ice, albedo, and partitioning of surface solar radiation in the
483 Pacific sector of Arctic Ocean during 1982-2009. *Journal of Geophysical Research: Oceans*, 121 (8): 5470-5486.
484 doi:10.1002/2016JC011831
- 485 Light, B. and Grenfell, T. C., et al., 2008. Transmission and absorption of solar radiation by Arctic sea ice during the melt
486 season. *Journal of Geophysical Research*, 113: C03023. doi:10.1029/2006JC003977
- 487 Light, B. and Maykut, G. A., et al., 2003. Effects of temperature on the microstructure of first-year Arctic sea ice. *Journal of*
488 *Geophysical Research: Oceans*, 108 (C2): 3051. doi:10.1029/2001JC000887
- 489 Light, B. and Maykut, G. A., et al., 2004. A temperature-dependent, structural-optical model of first-year sea ice. *Journal of*
490 *Geophysical Research*, 109: C06013. doi:10.1029/2003JC002164
- 491 Light, B. and Perovich, D. K., et al., 2015. Optical properties of melting first - year Arctic sea ice. *Journal of Geophysical*
492 *Research: Oceans*, 120 (11): 7657-7675. doi:10.1002/2015JC011163
- 493 Lindsay, R. and Schweiger, A., 2015. Arctic sea ice thickness loss determined using subsurface, aircraft, and satellite
494 observations. *The Cryosphere*, 9 (1): 269-283. doi:10.5194/tc-9-269-2015
- 495 Markus, T. and Stroeve, J. C., et al., 2009. Recent changes in Arctic sea ice melt onset, freezeup, and melt season length.
496 *Journal of Geophysical Research*, 114: C12024. doi:10.1029/2009JC005436
- 497 Mobley, C. D. and Cota, G. F., et al., 1998. Modeling Light Propagation in Sea Ice. *IEEE Transactions on Geoscience and*
498 *Remote Sensing*, 36 (5): 1743-1749. doi:10.1109/36.718642
- 499 Notz, D. and Worster, M. G., 2009. Desalination processes of sea ice revisited. *Journal of Geophysical Research*, 114 (C5).
500 doi:10.1029/2008JC004885
- 501 Parkinson, C. L. and Comiso, J. C., 2013. On the 2012 record low Arctic sea ice cover: Combined impact of preconditioning
502 and an August storm. *Geophysical Research Letters*, 40 (7): 1356-1361. doi:10.1002/grl.50349
- 503 Perovich, D. K., 2003. Complex yet translucent: the optical properties of sea ice. *Physica B: Condensed Matter*, 338 (1-4):
504 107-114. doi:10.1016/S0921-4526(03)00470-8
- 505 Perovich, D. and Light, B., et al., 2020. Changing ice and changing light: trends in solar heat input to the upper Arctic ocean
506 from 1988 to 2014. *Annals of Glaciology*, 61 (83): 401-407. doi:10.1017/aog.2020.62
- 507 Perron, C. and Katlein, C., et al., 2021. Development of a diffuse reflectance probe for in situ measurement of inherent
508 optical properties in sea ice. *The Cryosphere*, 15 (9): 4483-4500. doi:10.5194/tc-15-4483-2021
- 509 Petty, A. A. and Stroeve, J. C., et al., 2018. The Arctic sea ice cover of 2016: a year of record-low highs and
510 higher-than-expected lows. *The Cryosphere*, 12 (2): 433-452. doi:10.5194/tc-12-433-2018
- 511 Ricker, R. and Hendricks, S., et al., 2017. A weekly Arctic sea-ice thickness data record from merged CryoSat-2 and SMOS



- 512 satellite data. *The Cryosphere*, 11 (4): 1607-1623. doi:10.5194/tc-11-1607-2017
- 513 Rigor, I. G. and Wallace, J. M., 2004. Variations in the age of Arctic sea-ice and summer sea-ice extent. *Geophysical*
514 *Research Letters*, 31 (9): n/a-n/a. doi:10.1029/2004GL019492
- 515 Smedley, A. R. D. and Evatt, G. W., et al., 2020. Solar radiative transfer in Antarctic blue ice: spectral considerations,
516 subsurface enhancement, inclusions, and meteorites. *The Cryosphere*, 14 (3): 789-809. doi:10.5194/tc-14-789-2020
- 517 Smith, M. M. and Light, B., et al., 2022. Sensitivity of the Arctic Sea Ice Cover to the Summer Surface Scattering Layer.
518 *Geophysical Research Letters*, 49 (9): e2022GL098349. doi:10.1029/2022GL098349
- 519 Smith, R. C. and Baker, K. S., 1981. Optical properties of the clearest natural waters (200–800 nm). *Applied Optics*, 20 (2):
520 177. doi:10.1364/AO.20.000177
- 521 Stroeve, J. and Notz, D., 2018. Changing state of Arctic sea ice across all seasons. *Environmental research letters*, 13 (10):
522 103001. doi:10.1088/1748-9326/aade56
- 523 Timmermans, M. L., 2015. The impact of stored solar heat on Arctic sea ice growth. *Geophysical Research Letters*, 42 (15):
524 6399-6406. doi:10.1002/2015GL064541
- 525 Tschudi, M. A. and Meier, W. N., et al., 2020. An enhancement to sea ice motion and age products at the National Snow and
526 Ice Data Center (NSIDC). *The Cryosphere*, 14 (5): 1519-1536. doi:10.5194/tc-14-1519-2020
- 527 Tschudi, M. and Meier, W., et al., 2019. EASE-Grid Sea Ice Age, Version 4. [Indicate subset used]. Boulder, Colorado USA.
528 NASA National Snow and Ice Data Center Distributed Active Archive Center.. doi:10.5067/UTAV7490FEPB
- 529 Vancoppenolle, M. and Fichefet, T., et al., 2009. Simulating the mass balance and salinity of Arctic and Antarctic sea ice. 2.
530 Importance of sea ice salinity variations. *Ocean Modelling*, 27 (1-2): 54-69. doi:10.1016/j.ocemod.2008.11.003
- 531 Veyssière, G. and Castellani, G., et al., 2022. Under-Ice Light Field in the Western Arctic Ocean During Late Summer.
532 *Frontiers in Earth Science*, 9. doi:10.3389/feart.2021.643737
- 533 Wang, Q. and Lu, P., et al., 2020. Physical Properties of Summer Sea Ice in the Pacific Sector of the Arctic During 2008–
534 2018. *Journal of Geophysical Research: Oceans*, 125 (9). doi:10.1029/2020JC016371
- 535 Weeks, W. F. and Ackley, S. F., 1986. *The Growth, Structure, and Properties of Sea Ice*.
- 536 Yu, M. and Lu, P., et al., 2022. Impact of Microstructure on Solar Radiation Transfer Within Sea Ice During Summer in the
537 Arctic: A Model Sensitivity Study. *Frontiers in marine science*, 9 (861994). doi:10.3389/fmars.2022.861994
- 538 Zhang, J. and Schweiger, A., et al., 2018. Melt Pond Conditions on Declining Arctic Sea Ice Over 1979–2016: Model
539 Development, Validation, and Results. *Journal of Geophysical Research: Oceans*, 123 (11): 7983-8003.
540 doi:10.1029/2018JC014298

541